Quantifying the Spin-Orbital Entanglement in $5d^1$ Quantum Materials

V. García-Rojas and J. F. Pérez-Torres*

Escuela de Química, Universidad Industrial de Santander, Cra. 27-9, 680002 Bucaramanga, Colombia (Dated: November 25, 2025)

The spin-orbital entanglement in $5d^1$ transition metal ions embedded in double perovskites, where anomalous effective magnetic dipole moments are frequently observed, is quantified by the spin-orbital von Neumann entropy $\Delta S_{\rm vN}^{\rm SO}$. The framework is grounded on the relativistic crystal field theory, and is illustrated through a series of quantum materials: $A_2 \text{TaCl}_6$ (A = K, Rb), $A_2 \text{MgReO}_6$ (A = Ca, Sr, Ba) and $\text{Ba}_2 \text{NaOsO}_6$, all analyzed in their paramagnetic phases, alongside the ReF₆ molecular system. The entropies are derived from measurements of the optical d-d transitions $\Gamma_7(t_{2g}) \leftarrow \Gamma_8(t_{2g})$ and $\Gamma_8(e_g) \leftarrow \Gamma_8(t_{2g})$, and of the effective magnetic dipole moment $\mu_{\rm eff}$. It is demonstrated that, regardless of the system, the Kramers doublet $\Gamma_7(t_{2g})$ exhibits no spin-orbital von Neumann entropy. The entropies obtained for the relativistic crystal field states $\Gamma_8(t_{2g})$ and $\Gamma_8(e_g)$ uncover that, a larger effective magnetic dipole moment can be attributed to a grater spin-orbital entanglement, yet paradoxically not to a larger spin-orbit coupling constant.

I. INTRODUCTION

Quantum materials, so named for their exotic properties that emerge from the entanglement between different degrees of freedom, have been the subject of numerous investigations in recent years [1]. Among the most studied materials, are double perovskite oxides of heavy transition metals, which exhibit unusual magnetic behaviors such as unconventional magnetization, interplay between ferromagnetic and antiferromagnetic phases, multipolar domains, to name just a few [2–18]. These behaviours are mainly manifested in their anomalous heat capacities and their effective magnetic dipole moments [19]. For example, in perovskites with $5d^1$ transition metals, the magnetic dipole moment varies between 0.2 and 0.8 Bohr magnetons. These values are quite different from the expected value of 1.73 predicted by the spin-only magnetic moment. When the crystal field theory is furnished with the spin-orbit interaction, it results in a more complete model that predicts the splitting of the d orbitals in octahedral environments into three: the $\Gamma_8(t_{2q})$ orbitals, the $\Gamma_7(t_{2g})$ orbitals, and the $\Gamma_8(e_g)$ orbitals, consistent with the number of optical d-d transitions observed in these compounds: $\Delta_1 = \Gamma_8(e_q) \leftarrow \Gamma_8(t_{2q})$ and $\Delta_2 = \Gamma_7(t_{2q}) \leftarrow \Gamma_8(t_{2q})$. However, for the quadruplet ground state $\Gamma_8(t_{2q})$, a null magnetic dipole moment is predicted. The anomalous magnetic dipole moment, and thus the quantum properties that emerge from it, have been attributed to a strong spin-orbit coupling that goes beyond zeroth-order wave functions [20, 21]. In the strong crystal field approximation [20, 22], the optical dd transitions are described by $\Delta_1 = \xi_{nd}/2 + 10Dq$ and $\Delta_2 = 3\xi_{nd}/2$, where ξ_{nd} is the spin-orbit coupling constant and Dq is the strength of the crystal field. Thus, from the d-d transitions obtained by Resonant Inelastic X-ray Scattering (RIXS) measurements [12, 23], it is possible to calculate the parameters ξ_{nd} and Dq. The relatively high values of ξ_{nd} obtained for 5d metals, on the

order of 0.3 to 0.6 eV, confirm the strong spin-orbit coupling. Accordingly, it is widely accepted that a higher value of the spin-orbit coupling constant will result in greater entanglement between the orbital and spin degrees of freedom, and therefore a greater magnetic dipole moment. However, this hypothesis has not been confirmed. In this work, we will quantify the degree of spin-orbit entanglement for a family of $5d^1$ hexachlorides and double perovskite oxides using the von Neumann entropy, along with relativistic crystal field theory (RCFT) [24, 25]. The von Neumann entropy, important in quantum computing and quantum information theory [26], has been successfully used to quantify entanglement between different degrees of freedom, e.g. electronphonon [27], electron-nucleus [28, 29], electron-electron [30], orbital-orbital [31, 32], and spin-orbital [33–36] in various systems. The RCFT, which treats the spin-orbit interaction and the electrostatic crystal field on equal footing, predicts the correct number of d-d transitions and a non-zero magnetic dipole moment. We will demonstrate that the entropies correlate well with the effective magnetic dipole moment; consequently, both parameters ξ_{nd} and Dq, and the relativistic ratio p/q, characteristic of relativistic effects beyond the spin-orbit interaction. will play an important role in the magnetic properties of these compounds. The paper is organized as follows: In Sec. II the RCTF is briefly described. Then, in Sec. III the density matrix formalism is introduced in order to define the spin-orbital von Neumann entropy for the $nd^{1}(O_{h})$ relativistic crystal field states. In Sec. IV The developed model is benchmarked against $5d^1(O_h)$ transition metal hexachlorides and double perovskite oxides that exhibit quantum properties arising from strong spinorbit coupling. Finally, some conclusions and perspectives are outlined in Sec. V.

^{*} jfperezt@uis.edu.co

II. RELATIVISTIC CRYSTAL FIELD THEORY

In crystal field theory, the motion of a d-electron is represented by the Hamiltonian [20, 22, 37]

$$\hat{\mathcal{H}} = \hat{\mathcal{H}}_{atom} + \hat{\mathcal{H}}_{crystal-field} \tag{1}$$

where $\hat{\mathcal{H}}_{\text{crystal-field}}$ is the electrostatic crystal field potential [20, 22, 37]. In contrast to the standard crystal field theory, in its relativistic version $\hat{\mathcal{H}}_{\text{atom}}$ takes the Dirac form [24]:

$$\hat{\mathcal{H}}_{\text{atom}} = c\hat{\boldsymbol{\alpha}} \cdot \hat{\mathbf{p}} + \hat{\beta}mc^2 + V(r) \tag{2}$$

where $\hat{\alpha} = (\alpha_x, \alpha_y, \alpha_z)$ and $\hat{\beta}$ represent the Dirac matrices, c is the velocity of the light in the vacuum, \mathbf{p} and m are the momentum and the mass of the electron, respectively, and V(r) is the potential that contains the electron-nuclei and electron-inner electrons Coulomb interactions. For d-electrons, the eigenstates of \mathcal{H}_{atom} correspond to four-fold $nd_{3/2}$ and six-fold $nd_{5/2}$ energy degenerated spinors with magnetic quantum numbers $-3/2 \le m_j \le +3/2$ and $-5/2 \le m_j \le +5/2$, respectively [38]. When the atom is placed in a solid, the degeneracy is partially lifted because of the interaction with the surroundings, represented by $\mathcal{H}_{crystal-field}$. The interaction is mainly due to nearest neighbor atoms, the so-called ligands. In the case of the most common sixcoordinated octahedral symmetry, the six spinors $nd_{5/2}$ split into two sets of spinors which span the irreducible representations Γ_7 and Γ_8 of the double point group O_b' [39]. Since the $nd_{3/2}$ set also span the irreducible representation Γ_8 , the two sets of spinors belonging to Γ_8 mixes up [21]. Taking advace of the block diagonal matrix representation of the total Hamiltonian in the basis of symmetrized atomic Dirac spinors $\{nd_{3/2} \cup nd_{5/2}\}$, the crystal field eigenstates are found to be [25],

$$|\Gamma_7^a\rangle = \sqrt{\frac{1}{6}}|n-3-\frac{5}{2}\rangle - \sqrt{\frac{5}{6}}|n-3+\frac{3}{2}\rangle$$
 (3)

$$|\Gamma_7^b\rangle = \sqrt{\frac{1}{6}}|n-3+\frac{5}{2}\rangle - \sqrt{\frac{5}{6}}|n-3-\frac{3}{2}\rangle$$
 (4)

$$|\Gamma_{8\pm}^a\rangle = x_{\pm} \left(\sqrt{\frac{5}{6}}|n-3-\frac{5}{2}\rangle + \sqrt{\frac{1}{6}}|n-3+\frac{3}{2}\rangle\right) + y_{\pm}|n+2+\frac{3}{2}\rangle$$
 (5)

$$|\Gamma_{8\pm}^b\rangle = x_{\pm} \left(\sqrt{\frac{5}{6}}|n-3+\frac{5}{2}\rangle + \sqrt{\frac{1}{6}}|n-3-\frac{3}{2}\rangle\right)$$

$$-y_{\pm}|n+2-\frac{3}{2}\rangle\tag{6}$$

$$|\Gamma^c_{8\pm}\rangle = x_{\pm}|n-3-\frac{1}{2}\rangle + y_{\pm}|n+2-\frac{1}{2}\rangle \tag{7}$$

$$|\Gamma^d_{8\pm}\rangle = x_{\pm}|n-3+\frac{1}{2}\rangle - y_{\pm}|n+2+\frac{1}{2}\rangle \tag{8}$$

with expansion coefficients

$$x_{\pm} = \frac{\delta \pm \sqrt{\delta^2 + 1}}{\sqrt{\left(\delta \pm \sqrt{\delta^2 + 1}\right)^2 + 1}} \tag{9}$$

$$y_{\pm} = \frac{1}{\sqrt{\left(\delta \pm \sqrt{\delta^2 + 1}\right)^2 + 1}} \tag{10}$$

$$\delta = \frac{1}{2\sqrt{6}(p/q)} \left(\frac{5\xi_{nd}}{4Dq} + 1 \right) \tag{11}$$

effective magnetic dipole moment

$$\mu_{\text{eff}} = \sqrt{\frac{3}{4} \sum_{m_j = -3/2}^{3/2} (W_{m_j}^{\text{I}})^2}$$
 (12)

$$W_{\pm 1/2}^{\rm I} = \pm \frac{1}{2} \left(\frac{6}{5} x_{-}^2 + \frac{4}{5} y_{-}^2 + \frac{4\sqrt{6}}{5} x_{-} y_{-} \right) \mu_{\rm B}$$
 (13)

$$W_{\pm 3/2}^{\rm I} = \pm \frac{3}{2} \left(\frac{4}{5} y_{-}^2 - \frac{22}{15} x_{-}^2 - \frac{4\sqrt{6}}{45} x_{-} y_{-} \right) \mu_{\rm B}(14)$$

and energy levels

$$E(\Gamma_7) = \xi_{nd} - 4Dq$$

$$E(\Gamma_{8\pm}) = -\frac{\xi_{nd}}{4} + \left(1 \pm \sqrt{\left(\frac{5\xi_{nd}}{4Dq} + 1\right)^2 + 24(p/q)^2}\right) Dq$$
(16)

Here \pm stands for the lower (-) and upper (+) energy levels $\Gamma_8(t_{2g})$ and $\Gamma_8(e_g)$, respectively, see Figure 1. The ket notation $|n\kappa m_j\rangle$ has been used to represent the atomic spinors $d_{3/2}$ ($\kappa=+2$) and $d_{5/2}$ ($\kappa=-3$). The spin-orbit coupling constant ξ_{nd} , the crystal field strength Dq, and the relativistic ratio p/q, defined as [24]

$$\xi_{nd} = \frac{2}{5} \left(E(nd_{5/2}) - E(nd_{3/2}) \right) \tag{17}$$

$$Dq = \alpha \hbar c \frac{Z}{6a} \int_0^\infty |F_{nd_{5/2}}(r)|^2 r^4 dr$$
 (18)

$$p/q = \frac{\int_0^\infty F_{nd_{5/2}}(r)F_{nd_{3/2}}(r)r^4 dr}{\int_0^\infty |F_{nd_{5/2}}(r)|^2 r^4 dr}$$
(19)

can be obtained from the optical spectrum (d-d transitions) supplemented by magnetic susceptibility measurements [25] or ab-initio relativistic quantum chemistry calculations [24]. The radial functions $F_{nd_j}(r)$ correspond to the large component of the atomic spinors (see Appendix), α is the fine structure constant, \hbar is the reduced planck constant, $\mu_{\rm B}$ is the Bohr magneton, Z is the effective charge of the ligands, and a is the ligand-metal distance. We note that if we set p/q=1, the present formalism becomes equivalent to the full t_{2g} - e_g one-electron

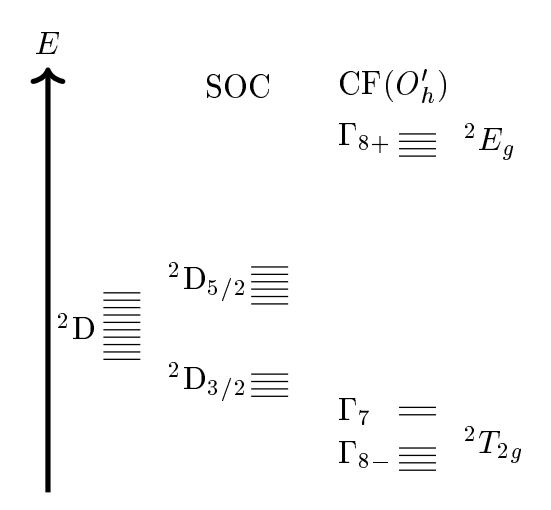


FIG. 1. Energy splitting of the $^2\mathrm{D}$ atomic state due to the spin-orbit coupling (SOC) and to the octahedral crystal field (CF) interactions. When the SOC is negligible the Γ_{8-} and Γ_{7} relativistic states, often referred to as $J_{\mathrm{eff}}=3/2$ and $J_{\mathrm{eff}}=1/2$, respectively, resemble the $^2T_{2g}$ non-relativistic crystal field state, see Ref. [21].

model developed in Ref. [21]. Using the Taylor expansion for $\sqrt{1+x}$ in Eq. (16) and assuming $10Dq \gg \xi_{nd}$ and p/q = 1, it can be shown that

$$\Delta_1 = E(\Gamma_{8+}) - E(\Gamma_{8-}) \approx \frac{1}{2}\xi_{nd} + 10Dq$$
 (20)

$$\Delta_2 = E(\Gamma_7) - E(\Gamma_{8-}) \approx \frac{3}{2} \xi_{nd} \tag{21}$$

which is known as the strong field approximation [40, 41]. Moreover, if $\xi_{nd} \rightarrow 0$, then both radial functions $F_{nd_{5/2}}(r)/r$ and $F_{nd_{3/2}}(r)/r$ are equal to the radial function $R_{nd}(r)$ of the Schrödinger orbitals $\psi_{n\ell m}(\mathbf{r}) =$ $R_{n\ell}(r)Y_{\ell m}(\theta\phi)$, and therefore p=q is obtained, see Eq. (19). Then, it follows that $E(\Gamma_{8-}) = E(\Gamma_7) = -4Dq$ and $E(\Gamma_{8+}) = +6Dq$, matching up with the energy levels $E(^2T_{2g})$ and $E(^2E_g)$ of the non-relativistic crystal field theory. Note that the pair of states $|\Gamma_i^a\rangle$ and $|\Gamma_i^b\rangle$, and $|\Gamma_i^c\rangle$ and $|\Gamma_i^d\rangle$, comprise Kramers doublets, i.e. $|\Gamma_i^b\rangle = -\hat{\mathcal{T}}|\Gamma_i^a\rangle$ and $|\Gamma_i^d\rangle = -\hat{\mathcal{T}}|\Gamma_i^c\rangle$, where $\hat{\mathcal{T}}: t \to -t \equiv$ $\hat{\mathcal{T}}|jm_i\rangle = (-1)^{j-m_j}|j-m_i\rangle$ is the time-reversal symmetry operator [38]. The theoretical framework described above has been used to analyze the optical and magnetic properties of $4d^1$ and $5d^1$ transition metal ions in cubic and tetragonal ligand fields [24, 25].

III. DENSITY MATRICES AND VON NEUMANN ENTROPY

Suppose we have a system described by the pure quantum state $|\Gamma_i\rangle$, then the density matrix operator associated to the state is given by [26]

$$\hat{\rho}_{\Gamma_i} = |\Gamma_i\rangle\langle\Gamma_i| \tag{22}$$

If the quantum state $|\Gamma_i\rangle$ contains orbital angular momentum ℓ and spin angular momentum s degrees of freedom, the partial traces for $\ell=2$ and s=1/2 Hilbert subspaces,

$$\operatorname{Tr}_{\ell}(\hat{\rho}_{\Gamma_{i}}) = \sum_{m_{\ell}=-2}^{2} \langle 2m_{\ell} | \hat{\rho}_{\Gamma_{i}} | 2m_{\ell} \rangle = \hat{\rho}_{\Gamma_{i}}^{(s)}$$
 (23)

$$\operatorname{Tr}_{s}\left(\hat{\rho}_{\Gamma_{i}}\right) = \sum_{m_{s}=-1/2}^{1/2} \langle \frac{1}{2} m_{s} | \hat{\rho}_{\Gamma_{i}} | \frac{1}{2} m_{s} \rangle = \hat{\rho}_{\Gamma_{i}}^{(\ell)} \quad (24)$$

define the reduced density matrix operators $\hat{\rho}_{\Gamma_i}^{(s)}$ and $\hat{\rho}_{\Gamma_i}^{(\ell)}$ associated to the spin and orbital angular momentum subspaces, respectively. Both reduced density matrix operators admit matrix representations in the eigenbasis $|\frac{1}{2}m_s\rangle$ and $|2m_\ell\rangle$, that is $\rho_{m'_sm_s}^{(s)}=\langle\frac{1}{2}m'_s|\hat{\rho}_{\Gamma_i}^{(s)}|\frac{1}{2}m_s\rangle$ and $\rho_{m'_\ell m_\ell}^{(\ell)}=\langle 2m'_\ell|\hat{\rho}_{\Gamma_i}^{(\ell)}|2m_\ell\rangle$, and share the same spectrum [28]. The spectrum of a reduced density matrix of dimension N is the set of eigenvalues $\{\lambda_i\}$ that satisfy $0\leq \lambda_i\leq 1$ and $\sum_{i=1}^N \lambda_i=1$. If the spectrum is such that $\lambda_i=\delta_{ij}$, then the quantum state is said to be separable; otherwise, the quantum state is said to be entangled. Finally, the von Neumann entropy, defined as

$$S_{\text{vN}} = -\text{Tr}(\hat{\rho}\log_2\hat{\rho}) = -\sum_i \lambda_i \log_2(\lambda_i)$$
 (25)

quantifies the strength of entanglement between the two halfspaces. It turns out that, for our particular case of $nd^1(O_h)$ systems, the matrix representation of the reduced density matrices $\hat{\rho}_{\Gamma_i}^{(s)}$ of the spin halfspace is diagonal in the basis of Pauli eigenvectors $\{|\alpha\rangle=|\frac{1}{2}+\frac{1}{2}\rangle, |\beta\rangle=|\frac{1}{2}-\frac{1}{2}\rangle\}$. Therefore, the eigenvalues required to obtain the von Neumann entropies of the quantum states Γ_i turn out to be:

$$\lambda_1(\Gamma_7^a) = \langle \alpha | \hat{\rho}_{\Gamma_7 a}^{(s)} | \alpha \rangle = \frac{2}{3}$$
 (26)

$$\lambda_2(\Gamma_7^a) = \langle \beta | \hat{\rho}_{\Gamma_{7a}}^{(s)} | \beta \rangle = \frac{1}{3}$$
 (27)

$$\lambda_1(\Gamma_{8+}^a) = \langle \alpha | \hat{\rho}_{\Gamma_{8+a}}^{(s)} | \alpha \rangle$$

$$= \frac{2}{15}x_{\pm}^2 + \frac{1}{5}y_{\pm}^2 - \frac{2\sqrt{6}}{15}x_{\pm}y_{\pm}$$
 (28)

$$\lambda_2(\Gamma_{8\pm}^a) = \langle \beta | \hat{\rho}_{\Gamma_{8\pm a}}^{(s)} | \beta \rangle$$

$$= \frac{13}{15}x_{\pm}^2 + \frac{4}{5}y_{\pm}^2 + \frac{2\sqrt{6}}{15}x_{\pm}y_{\pm} \tag{29}$$

$$\lambda_1(\Gamma_{8\pm}^c) = \langle \alpha | \hat{\rho}_{\Gamma_{8\pm}c}^{(s)} | \alpha \rangle$$

$$= \frac{2}{5}x_{\pm}^2 + \frac{3}{5}y_{\pm}^2 - \frac{2\sqrt{6}}{5}x_{\pm}y_{\pm} \tag{30}$$

$$\lambda_2(\Gamma^c_{8\pm}) = \langle \beta | \hat{\rho}^{(s)}_{\Gamma_{8\pm c}} | \beta \rangle$$

$$= \frac{3}{5}x_{\pm}^2 + \frac{2}{5}y_{\pm}^2 + \frac{2\sqrt{6}}{5}x_{\pm}y_{\pm} \tag{31}$$

The eigenvalues for the remaining states can be obtained using the time-reversal symmetry operator, e.g. $\lambda_1(\Gamma_7^b)$ =

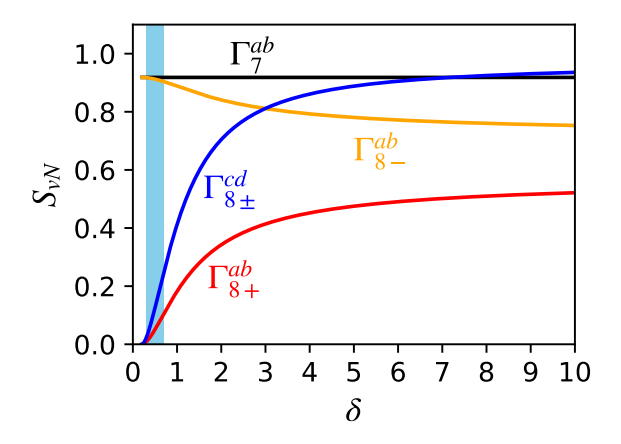


FIG. 2. von Neumann entropy S_{vN} of the Γ_7 and Γ_8 states of nd^1 ions in octahedral crystal fields as a function of δ . The shadow rectangle indicates the typical values of δ for $5d^1(O_h)$ systems $(0.3 \le \delta \le 0.7)$.

 $\langle \alpha | \hat{\mathcal{T}}^{-1} \hat{\mathcal{T}} | \rho_{\Gamma_{c}^{b}}^{(s)} | \hat{\mathcal{T}} \hat{\mathcal{T}}^{-1} | \alpha \rangle$. Notice that $\lambda_{1}(\Gamma_{i}) + \lambda_{2}(\Gamma_{i}) = 1$. As expected from Eqs. 3 and 4, the von Neumann entropy for the crystal field states Γ_7^a and Γ_7^b is constant: $S_{\text{vN}}(\Gamma_7^{ab}) = -(1/3)\log_2(1/3) - (2/3)\log_2(2/3) = 0.918,$ that is, it is the same for any compound $nd^1(O_h)$. Since the parameter δ contains all the experimental quantities Dq, ξ_{nd} and p/q, it is convenient to represent the entropies $S_{\rm vN}(\Gamma_i)$ as a function of δ . Figure 2 shows the von Neumann entropy for the Kramers doublets $(\Gamma_{8\pm}^a, \Gamma_{8\pm}^b)$, $(\Gamma_{8\pm}^c, \Gamma_{8\pm}^d)$, and (Γ_7^a, Γ_7^b) . Surprisingly, $S_{vN}(\Gamma_{8-}^{cd}) = S_{vN}(\Gamma_{8+}^{cd})$, i.e. two Kramers doublets from different energy levels share the same degree of spin-orbital entanglement. In general, $S_{\rm vN}(\Gamma_{8-}^{ab})$ barely changes with δ , while $S_{\rm vN}(\Gamma^{cd}_{8+})$ and $S_{\rm vN}(\Gamma^{ab}_{8+})$ change abruptly. In the limit of zero spin-orbit interaction, i.e. $\xi_{nd} \to 0$, we obtain p = q, $\delta = 1/2\sqrt{6}$ (see Eqs. (19) and (11)), $S_{\rm vN}(\Gamma_7^{ab}) = S_{\rm vN}(\Gamma_{8-}^{ab}) = 0.918$ and $S_{\rm vN}(\Gamma^{cd}_{8\pm}) = S_{\rm vN}(\Gamma^{ab}_{8\pm}) = 0$. This can be understood as follows: for zero spin-orbit interaction, the relativistic crystal field states $|\Gamma_i\rangle$ resemble, up to a global phase, the Ballhausen's crystal field spin-orbitals [20], see Table I. It immediately follows that only the states Γ^{ab}_{8-} and Γ^{ab}_{7} are entangled (non-separable) states. Indeed, von Neumann entropy quantifies our ignorance about the quantum state of a system. For instance, if the system is described by the state $\Gamma_{8^c}(t_{2g})$, we know with certainty that the electron is represented by the crystal field orbital t_{2q}^- with spin state α , and therefore $S_{\rm vN}(\Gamma_{8^c}(t_{2g}))=0$. Additionally, the eigenvalues of the density matrices of the entangled states are easily obtained: $\lambda_1(\Gamma_{8^a}) = \lambda_2(\Gamma_{7^a}) = 1/3$ and $\lambda_2(\Gamma_{8^a}) = \lambda_1(\Gamma_{7^a}) = 2/3$, in agreement with our early results. Obviously, such entanglement can not be attributed to the spin-orbit interaction but to the symmetry point group. Therefore, in order to quantify the spin-orbital entanglement, we define the spin-orbital von

Neumann entropy for the state Γ_i as

$$\Delta S_{\text{vN}}^{\text{SO}}(\Gamma_i) = S_{\text{vN}}(\Gamma_i) - S_{\text{vN}}^{(\xi_{nd}=0)}(\Gamma_i)$$
 (32)

Thus, the spin-orbit interaction does not produce any entropy in the Kramers doublet Γ_7 . Only the Kramers doublets Γ_8 are influenced by the spin-orbit interaction, with negative spin-orbital entropy for the Kramers doublet Γ_{8-}^{ab} as the spin-orbit interaction is turned on. The

TABLE I. Correlation between Ballhausen's spin-orbitals [20] and relativistic crystal field states (RCFS) for $\xi_{nd} \to 0$. For a detailed description of the spin-orbitals see page 118 of Ballhausen's Book [20].

Ballhausen's spin-orbitals	RCFS
$\Gamma_{8^a}(t_{2g}) = \sqrt{1/3}(-\sqrt{2}t_{2g}^0\beta + t_{2g}^+\alpha)$	
$\Gamma_{8b}(t_{2g}) = \sqrt{1/3}(-\sqrt{2}t_{2g}^0\alpha - t_{2g}^-\beta)$	Γ_{8-}^{b}
$\Gamma_{8^c}(t_{2g}) = t_{2g}^- \alpha$	$-\Gamma_{8-}^{c}$
$\Gamma_{8^d}(t_{2g}) = -t_{2g}^+ \beta$	Γ_{8-}^d
$\Gamma_{7a}(t_{2g}) = \sqrt{1/3}(t_{2g}^0\beta + \sqrt{2}t_{2g}^+\alpha)$	$-\Gamma_7^a$
$\Gamma_{7b}(t_{2g}) = \sqrt{1/3}(-t_{2g}^0\alpha + \sqrt{2}t_{2g}^-\beta)$	Γ_7^b
$\Gamma_{8^a}(e_g) = e_g^b \beta$	Γ_{8+}^a
$\Gamma_{8b}(e_g) = -e_g^b \alpha$	$-\Gamma_{8+}^b$
$\Gamma_{8^c}(e_g) = e_g^a \mathring{eta}$	Γ_{8+}^c
$\Gamma_{8^d}(e_g) = -e_g^a \alpha$	$-\Gamma^d_{8+}$

asymptotic values of $S_{\rm vN}$ for large δ , i.e. $Dq \to 0$, are easily obtained from the limits

$$\lim_{D_{\sigma} \to 0} x_{-} = \lim_{D_{\sigma} \to 0} y_{+} = 0 \tag{33}$$

$$\lim_{Dq \to 0} x_{-} = \lim_{Dq \to 0} y_{+} = 0$$

$$\lim_{Dq \to 0} x_{+} = \lim_{Dq \to 0} y_{-} = 1$$
(33)

which give rise to the asymptotic entropies

$$S_{\text{vN}}(\Gamma_{8-}^{ab}) = -\frac{1}{5}\log_2(\frac{1}{5}) - \frac{4}{5}\log_2(\frac{4}{5})$$

= 0.722 (35)

$$S_{\text{vN}}(\Gamma_{8+}^{ab}) = -\frac{2}{15}\log_2(\frac{2}{15}) - \frac{13}{15}\log_2(\frac{13}{15})$$
$$= 0.567 \tag{36}$$

$$S_{\text{vN}}(\Gamma_{8\pm}^{cd}) = -\frac{2}{5}\log_2(\frac{2}{5}) - \frac{3}{5}\log_2(\frac{3}{5})$$

= 0.971 (37)

Remarkably, none of the states reaches the maximum entanglement $\lambda_1^{\text{max}} = \lambda_2^{\text{max}} = 1/2$ and $S_{\text{vN}}^{\text{max}} = 1$. From the monotonic behavior of $\Delta S_{\text{vN}}^{\text{SO}}$ with δ , follows that the spin-orbit entanglement increases with the spin-orbit coupling constant ξ_{nd} , as expected, but decreases with the crystal field strength Dq and with the ratio p/q.

IV. SPIN-ORBITAL VON NEUMANN ENTROPY IN QUANTUM MATERIALS

In this section we study the spin-orbital entanglement in a set of quantum materials through the spinorbital von Neumann entropy. The family of hexachlorides A_2 TaCl₆ (A = K, Rb) and double perovskite oxides

TABLE II. Reported d-d optical transitions Δ_1 : $\Gamma_8(e_g) \leftarrow \Gamma_8(t_{2g})$, Δ_2 : $\Gamma_7(t_{2g}) \leftarrow \Gamma_8(t_{2g})$, and effective magnetic dipole moments μ_{eff} employed in this work.

	Δ_1/eV	Δ_2/eV	$\mu_{ m eff}/\mu_{ m B}$
K_2 TaCl ₆	3.20 (ref [5])	0.40 (ref [5])	0.30 (ref [5])
Rb_2TaCl_6	3.20 (ref [5])	0.40 (ref [5])	0.27 (ref [5])
ReF_{6}	3.65 (ref [41])	0.62 (ref [41])	0.25 (ref [42])
Ca_2MgReO_6	4.95 (ref [12])	0.545(ref [12])	_
Sr_2MgReO_6	4.91 (ref [12])	0.535(ref [12])	_
Ba_2MgReO_6	4.56 (ref [12])	0.52 (ref [12])	0.68 (ref [6])
Ba_2NaOsO_6	4.86 (ref [11])	0.51 (ref [11])	0.677 (ref [43])

 A_2 MgReO₆ (A = Ca, Sr, Ba) and Ba_2 NaOsO₆, are employed as benchmarks. The ReF₆ molecular system is analyzed as well. We should point out that the local symmetry of A_2 MgReO₆ and Ba₂NaOsO₆ is D_{4h} and not O_h , due to dynamic Jahn-Teller effect [11, 12]. However, the spliting of the ground state $\Gamma_8(t_{2g})$ is one order of magnitude smaller than the spin-orbit coupling, being $\Delta_{\rm JT} \approx 0.030 \ {\rm eV}$ for $A_2{\rm MgReO_6}$ and similar for Ba₂NaOsO₆. On the other hand, the RIXS spectra at room temperature reveal a four-fold degenerated $\Gamma_8(t_{2q})$ ground state for the family A_2 TaCl₆ (A = K, Rb, Cs) [5]. Therefore, assuming octahedral symmetry in all cases is safe. Table II gathers the reported experimental optical d-d transition energies and effective magnetic dipole moments used in this work. The calculated spinorbit coupling constants ξ_{5d} , crystal field strengths Dq, and ratios p/q, were obtained according to the protocol described in ref [25], and are reported in Table III together with the spin-orbital von Neumann entropies $\Delta S_{\rm vN}^{\rm SO}$. Because of the lack of reported magnetic susceptibility measurements for Ca₂MgReO₆ and Sr₂MgReO₆, ab-initio relativistic quantum chemistry calculations were carried out for atomic Re⁶⁺ in order to obtain the ratio p/q = 0.963 as reported in ref [24]. In general, the

TABLE III. Spin-orbit coupling constant ξ_{5d} , crystal field stength Dq, relativistic ratio p/q, and spin-orbital von Neumann entropies $\Delta S_{\rm vN}^{\rm SO}$ of crystal field states of $5d^1$ transition metal ions in octahedral environments. The values are obtained using the effective magnetic dipole moments and energies presented in the Table II, see Appendix. *Values obtained from ab-initio relativistic quantum chemistry calculations at the Dirac-Hartree-Fock level [24].

	ξ_{5d}/eV	Dq/eV	p/q		$\Delta S_{ m vN}^{ m SO}$	
				Γ_{8-}^{ab}	Γ_{8+}^{ab}	$\Gamma^{cd}_{8\pm}$
K_2 TaCl ₆	0.211	0.293	1.046	-0.0020	0.0205	0.0522
Rb_2TaCl_6	0.195	0.289	1.066	-0.0016	0.0170	0.0435
ReF_6	0.232	0.299	1.180	-0.0013	0.0148	0.0379
Ca_2MgReO_6	0.386	0.483	0.963*	-0.0034	0.0321	0.0804
Sr_2MgReO_6	0.380	0.479	0.963*	-0.0033	0.0316	0.0794
Ba_2MgReO_6	0.584	0.498	0.787	-0.0115	0.0882	0.2112
${ m Ba_2NaOsO_6}$	0.614	0.538	0.778	-0.0114	0.0874	0.2094

spin-orbit coupling constants obtained here follow the expected trend with the atomic number Z for isoelectronic

ions, i.e. $\xi_{5d}(\mathrm{Ta}^{4+}) < \xi_{5d}(\mathrm{Re}^{6+}) < \xi_{5d}(\mathrm{Os}^{7+})$. To contrast the results, we compare the magnetic moments of K_2TaCl_6 and Ba_2NaOsO_6 , as reported in Table 2, with the spin-orbit coupling values calculated in Table 3. For this pair, it seems to be a clear correlation indicating that greater spin-orbit coupling corresponds to a higher magnetic moment. However, when we examine the pairs K₂TaCl₆ and ReF₆, a different trend emerges; although the magnetic moment of K₂TaCl₆ is greater than that of ReF₆, the calculated spin-orbit coupling for ReF₆ is actually higher than that for K₂TaCl₆. However, within the families A_2 TaCl₆ and A_2 MgReO₆, it is found the spinorbit interaction takes precedence over the crystal field strength, since the spin-orbital von Neumann entropy follows the expected behavior with ξ_{5d} but not with Dq. Thus, in general, none of the crystal field parameters correlates with the entropy and therefore with the degree of spin-orbital entanglement. Interestingly, despite the different spin-orbit coupling constants for Ba₂MgReO₆ and Ba₂NaOsO₆, the von Neumann entropies reveal comparable, if not equal, entanglement for both perovskites. This is so because the increase in ξ_{5d} is offset by the increase in Dq at almost equal p/q, equilibrating the δ values for both perovskites. This result confirms our expectation that, to quantify the spin-orbital entanglement, all the relativistic crystal field parameters must be taken into account. This is achieved through the spin-orbital von Neumann entropy. Moreover, a notable correlation between the entropies and the effective magnetic dipole moment is observed from Tables II and III. This can be better appreciated from Figure 3, where the effective magnetic dipole moment and the spin-orbital von Neumann entropies are plotted against the parameter δ . Note that δ contains all the relativistic crystal field parameters, see eqn (11). Thus, the relativistic ratio and the crystal field strength also play a role in the entanglement between the orbital and spin degrees of freedom and can not be ignored. This findings confirm that the anomalous effective magnetic dipole moment, attributed to the strong spin-orbital entanglement, is better characterized by the spin-orbital von Neumann entropy rather than the spin-orbit coupling constant. We should mention that the vanishing of the effective magnetic dipole moment when $\delta \to 1/2\sqrt{6}$ must be associated to $\xi_{nd}/Dq \to 0$ instead of $\xi_{nd} \to 0$. This is because, as the spin-orbit coupling constant decreases, on the order of $k_{\rm B}T\approx 0.0259~{\rm eV}$, the van Vleck magnetic susceptibility [44] caused by the virtual transitions between the states Γ_{8-} and Γ_{7} becomes significant, for which Eq. (12) is not longer valid. Finally, because of the entanglement between the spin, orbital, and lattice degrees of freedom [12, 16, 18], a small effect of the temperature on the entropies should be expected.

V. CONCLUSIONS AND OUTLOOK

In conclusion, it has established a framework that allows us to quantify the spin-orbital entanglement in the

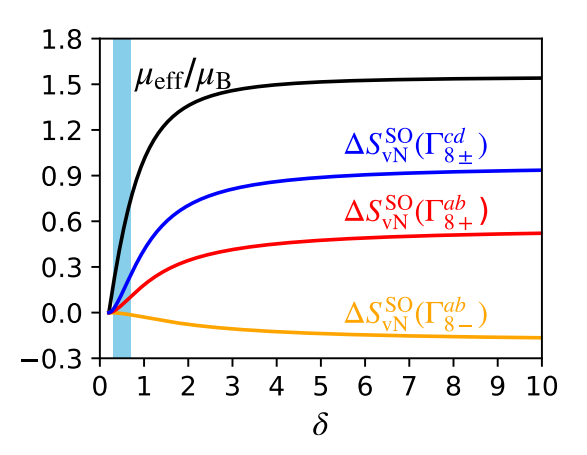


FIG. 3. Effective magnetic dipole moment $\mu_{\rm eff}$ and spinorbital von Neumann entropies $\Delta S_{\rm vN}^{\rm SO}$ for nd^1 ions in octahedral crystal fields as a function of the parameter δ . The shadow rectangle indicates the typical values of δ for $5d^1(O_h)$ systems $(0.3 \le \delta \le 0.7)$.

quantum states of $nd^1(O_h)$ systems from optical and magnetic measurements. The method is based on the von Neumann entropy and on the relativistic crystal field theory, yielding the spin-orbital von Neumann (SOvN) entropy as the key quantity. A family of $5d^1$ transition metal hexachlorides and double perovskite oxides, exhibiting properties of quantum materials, was analyzed. The molecular system ReF₆ was analyzed as well. It

was discovered that the effective magnetic dipole moment μ_{eff} correlates well with the SOvN entropy, but not necessarily with the spin-orbit coupling constant ξ_{5d} or the crystal field strength Dq. In general, the quadruplet ground state of these systems is characterized by two well-distinct Kramers doublets: one doublet is weakly entangled showing negative SOvN entropy $\Delta S_{\rm vN}^{\rm SO}(\Gamma_{8-}^{ab}) \lesssim 0$, while the other is strongly entangled with an SOvN entropy equal to that of one of the Kramers doublets of the second excited state, i.e. $\Delta S_{\rm vN}(\Gamma_{8-}^{cd}) = \Delta S_{\rm vN}(\Gamma_{8+}^{cd}) > 0$. The second Kramers doublet of the second excited state exhibits a moderate entanglement $\Delta S_{\rm vN}(\Gamma_{8+}^{ab}) \gtrsim 0$. Curiously, the first excited state of these systems lacks SOvN entropy $\Delta S_{\rm vN}^{\rm SO}(\Gamma_7^{ab}) = 0$. The phenomenological framework developed here should be considered as a bridge between experiment and theory. It would be interesting to derive the corresponding SOvN entropy from ab initio and density functional theory calculations [11, 45-49], in particular employing the ab initio ligand field theory [50–55]. We envision that with more experimental data available, new features will emerge from the SOvN entropy. An important prospect for the von Neumann entropy, along with the relativistic crystal field theory, lies in its possible extensions to more complex scenarios like spin-orbital-lattice and many-electron entangled systems, including other symmetries like tetragonal or trigonal crystal fields.

Appendix A: Appendix

1. Density matrix operators of crystal field states

The density matrix operators for the crystal field states of $nd^1(O_h)$ ions in the basis of atomic d-spinors are

$$\begin{split} \hat{\rho}_{\Gamma^{\alpha}_{7}} &= \frac{5}{6}|n-3\frac{3}{2}\rangle\langle n-3\frac{3}{2}| + \frac{1}{6}|n-3-\frac{5}{2}\rangle\langle n-3-\frac{5}{2}| - \frac{\sqrt{5}}{6}|n-3\frac{3}{2}\rangle\langle n-3-\frac{5}{2}| - \frac{\sqrt{5}}{6}|n-3-\frac{5}{2}\rangle\langle n-3\frac{3}{2}| \\ \hat{\rho}_{\Gamma^{\alpha}_{8\pm}} &= x_{\pm}^{2} \left(\frac{5}{6}|n-3-\frac{5}{2}\rangle\langle n-3-\frac{5}{2}| + \frac{1}{6}|n-3\frac{3}{2}\rangle\langle n-3\frac{3}{2}| + \sqrt{\frac{5}{6}}|n-3-\frac{5}{2}\rangle\langle n-3\frac{3}{2}| + \sqrt{\frac{5}{6}}|n-3\frac{3}{2}\rangle\langle n-3-\frac{5}{2}|\right) \\ &+ y_{\pm}^{2}|n2\frac{3}{2}\rangle\langle n2\frac{3}{2}| + x_{\pm}y_{\pm} \left(\sqrt{\frac{5}{6}}|n-3-\frac{5}{2}\rangle\langle n2\frac{3}{2}| + \sqrt{\frac{1}{6}}|n-3\frac{3}{2}\rangle\langle n2\frac{3}{2}|\right) \\ &+ x_{\pm}y_{\pm} \left(\sqrt{\frac{5}{6}}|n2\frac{3}{2}\rangle\langle n-3-\frac{5}{2}| + \sqrt{\frac{1}{6}}|n2\frac{3}{2}\rangle\langle n-3\frac{3}{2}|\right) \\ \hat{\rho}_{\Gamma^{c}_{8\pm}} &= x_{\pm}^{2}|n-3-\frac{1}{2}\rangle\langle n-3-\frac{1}{2}| + y_{\pm}^{2}|n2-\frac{1}{2}\rangle\langle n2-\frac{1}{2}| + x_{\pm}y_{\pm}|n-3-\frac{1}{2}\rangle\langle n2-\frac{1}{2}| \\ &+ x_{\pm}y_{\pm}|n2-\frac{1}{2}\rangle\langle n-3-\frac{1}{2}| \end{split} \tag{A3}$$

The expansion coefficients x_{\pm} and y_{\pm} are obtained from experimental measurements, see main text. The remaining density matrix operators can be obtained with the help of the time-reversal operator, i.e. $\hat{\rho}_{\Gamma_7^b} = \hat{\mathcal{T}}\hat{\rho}_{\Gamma_8^a}\hat{\mathcal{T}}$, $\hat{\rho}_{\Gamma_{8\pm}^b} = \hat{\mathcal{T}}\hat{\rho}_{\Gamma_{8\pm}^a}\hat{\mathcal{T}}$, and $\hat{\rho}_{\Gamma_{8\pm}^d} = \hat{\mathcal{T}}\hat{\rho}_{\Gamma_{8\pm}^c}\hat{\mathcal{T}}$.

2. Atomic d-spinors

The atomic Dirac spinors read [38]

$$\Psi_{n\kappa m_j}(r\theta\phi) = \frac{1}{r} \begin{bmatrix} F_{n\kappa}(r)\Omega_{\kappa m_j}(\theta\phi) \\ iG_{n\kappa}(r)\Omega_{-\kappa m_j}(\theta\phi) \end{bmatrix}$$
(A4)

where r, θ and ϕ are the spherical polar coordinates, and $F_{n\kappa}(r)$ and $G_{n\kappa}(r)$ are the large and small radial components, respectively. The sphreical spinors $\Omega_{\kappa m_j}(\theta\phi) = \langle \theta\phi | km_j \rangle$ are defined in terms of the spherical harmonics

 $Y_{\ell m_{\ell}}(\theta \phi) = \langle \theta \phi | \ell m_{\ell} \rangle$ by

$$|\kappa m_j\rangle = \begin{bmatrix} \operatorname{sgn}(-\kappa)\sqrt{\frac{\kappa + \frac{1}{2} - m_j}{2\kappa + 1}} |\ell, m_j - \frac{1}{2}\rangle \\ \sqrt{\frac{\kappa + \frac{1}{2} + m_j}{2\kappa + 1}} |\ell, m_j + \frac{1}{2}\rangle \end{bmatrix}$$
(A5)

Neglecting the small component $G_{n\kappa}(r) \approx 0$ within the approximation $F_{nd_{5/2}}(r) \approx F_{nd_{3/2}}(r)$, and using the Pauli eigenvectors

$$|\alpha\rangle = \begin{bmatrix} 1\\0 \end{bmatrix}, \quad |\beta\rangle = \begin{bmatrix} 0\\1 \end{bmatrix}$$
 (A6)

the atomic $nd_{3/2}$ -spinors and $nd_{5/2}$ -spinors can be recast as

$$|n2 - \frac{3}{2}\rangle = \sqrt{\frac{1}{5}}|nd_{-1}\beta\rangle - \sqrt{\frac{4}{5}}|nd_{-2}\alpha\rangle \quad (A7)$$

$$|n2-\frac{1}{2}\rangle = \sqrt{\frac{2}{5}}|nd_0\beta\rangle - \sqrt{\frac{3}{5}}|nd_{-1}\alpha\rangle$$
 (A8)

$$|n2+\frac{1}{2}\rangle = \sqrt{\frac{3}{5}}|nd_{+1}\beta\rangle - \sqrt{\frac{2}{5}}|nd_0\alpha\rangle \qquad (A9)$$

$$|n2+\frac{3}{2}\rangle = \sqrt{\frac{4}{5}}|nd_{+2}\beta\rangle - \sqrt{\frac{1}{5}}|nd_{+1}\alpha\rangle \quad (A10)$$

and

$$|n-3-\frac{3}{2}\rangle = \sqrt{\frac{4}{5}}|nd_{-1}\beta\rangle + \sqrt{\frac{1}{5}}|nd_{-2}\alpha\rangle$$
 (A12)

(A11)

 $|n-3-\frac{5}{2}\rangle = |nd-2\beta\rangle$

$$|n-3-\frac{1}{2}\rangle = \sqrt{\frac{3}{5}}|nd_0\beta\rangle + \sqrt{\frac{2}{5}}|nd_{-1}\alpha\rangle \quad (A13)$$

$$|n-3+\frac{1}{2}\rangle = \sqrt{\frac{2}{5}}|nd_{+1}\beta\rangle + \sqrt{\frac{3}{5}}|nd_0\alpha\rangle$$
 (A14)

$$|n-3+\frac{3}{2}\rangle=\sqrt{\frac{1}{5}}|nd_{+2}\beta\rangle+\sqrt{\frac{4}{5}}|nd_{+1}\alpha\rangle \quad (A15)$$

$$|n-3+\frac{5}{2}\rangle = |nd_{+2}\alpha\rangle \tag{A16}$$

respectively. Inserting the above form of the atomic nd_j -spinors into the matrix density operators of the relativistic crystal field states and tracing out the orbital angular momentum degree of freedom, the matrix representation of the reduced density matrices for the spin halfspace and thereof the eigenvalues required for the von Neumann entropy, are straightforwardly obtained.

3. Calculation of crystal field parameters

First, the parameter δ is obtained by fitting the equation

$$(\mu_{\text{eff}}/\mu_{\text{B}})^{2} = \frac{3}{200} \left(5 + \frac{(\delta - \sqrt{\delta^{2} + 1})^{2} - 1 + 4\sqrt{6}(\delta - \sqrt{\delta^{2} + 1})}{(\delta - \sqrt{\delta^{2} + 1})^{2} + 1} \right)^{2} + \frac{1}{150} \left(\frac{18 - 33(\delta - \sqrt{\delta + 1})^{2} - 2\sqrt{6}(\delta - \sqrt{\delta^{2} + 1})}{(\delta - \sqrt{\delta^{2} + 1})^{2} + 1} \right)^{2}$$
(A17)

to the known effective magnetic dipole moment μ_{eff} . Then, the parameters derived from the relativistic crystal field theory are calculated using the following equations:

$$Dq = \left(1 + \frac{\delta}{\sqrt{\delta^2 + 1}}\right) \frac{\Delta_1}{12} - \frac{\Delta_2}{6} \qquad (A18)$$

$$\xi_{nd} = \frac{2\delta\Delta_1}{5\sqrt{\delta^2 + 1}} - \frac{4}{5}Dq \tag{A19}$$

$$p/q = \frac{1}{2\delta\sqrt{6}} \left(\frac{5\xi_{nd}}{4Dq} + 1 \right) \tag{A20}$$

The obtained crystal field strength Dq, spin-orbit coupling constant ξ_{nd} , and relativistic ratio p/q, reproduce the experimental d-d optical transitions energies Δ_1 and Δ_2 , and effective magnetic dipole moment $\mu_{\rm eff}$, according to the relativistic crystal field theory.

ACKNOWLEDGMENTS

There is no funding to report in this work. J. F. Pérez-Torres conceived the original idea, developed the theoretical framework, and performed the calculations. V. García-Rojas located published experimental data and interpreted the results. All authors discussed the results and contributed to the final version of the manuscript.

DATA AVAILABITY

All the numerical results shown in this work can be obtained straightfordwardly from the formulas presented in the main text following the protocol described in the Appendix.

- R. Cava, N. de Leon, and W. Xie, Introduction: Quantum Materials, Chem. Rev. 121, 2777 (2021).
- [2] A. S. Erickson, S. Misra, G. J. Miller, R. R. Gupta, Z. Schlesinger, W. A. Harrison, J. M. Kim, and I. R. Fisher, Ferromagnetism in the Mott Insulator Ba₂NaOsO₆, Phys. Rev. Lett. 99, 016404 (2007).
- [3] H. J. Xiang and M.-H. Whangbo, Cooperative effect of electron correlation and spin-orbit coupling on the electronic and magnetic properties of Ba₂NaOsO₆, Phys. Rev. B 75, 052407 (2007).
- [4] G. Chen, R. Pereira, and L. Balents, Exotic phases induced by strong spin-orbit coupling in ordered double perovskites, Phys. Rev. B 82, 174440 (2010).
- [5] H. Ishikawa, T. Takayama, R. K. Kremer, J. Nuss, R. Dinnebier, K. Kitagawa, K. Ishii, and H. Takagi, Ordering of hidden multipoles in spin-orbit entangled 5d¹ Ta chlorides, Phys. Rev. B 100, 045142 (2019).
- [6] D. Hirai and Z. Hiroi, Successive Symmetry Breaking in a J_{eff} = 3/2 Quartet in the Spin-Orbit Coupled Insulator Ba₂MgReO₆, J. Phys. Soc. Jpn. 88, 064712 (2019).
- [7] D. I. Khomskii and S. V. Streltsov, Orbital Effects in Solids: Basics, Recent Progress, and Opportunities, Chem. Rev. 121, 2992 (2021).
- [8] L. T. Nguyen and R. J. Cava, Hexagonal perovskites as quantum materials, Chem. Rev. 121, 2935 (2021).
- [9] R. Cong, E. Garcia, P. C. Forino, A. Tassetti, G. Allodi, A. P. Reyes, P. M. Tran, P. M. Woodward, C. Franchini, S. Sanna, and V. F. Mitrović, Effects of charge doping on Mott insulator with strong spin-orbit coupling, Ba₂Na_{1-x}CaxOsO₆, Phys. Rev. Mater. 7, 084409 (2023).
- [10] J. Pásztorová, A. M. Tehrani, I. Živković, N. A. Spaldin, and H. M. Rønnow, Experimental and theoretical thermodynamic studies in Ba₂MgReO₆—the ground state in the context of Jahn-Teller effect, J. Phys.: Condens. Matter 35, 245603 (2023).
- [11] S. Agrestini, F. Borgatti, P. Florio, J. Frassineti, D. F. Mosca, Q. Faure, B. Detlefs, C. Sahle, S. Francoual, J. Choi, M. Garcia-Fernandez, K.-J. Zhou, V. Mitrović, P. Woodward, G. Ghiringhelli, C. Franchini, F. Boscherini, S. Sanna, , and M. M. Sala, Origin of Magnetism in a Supposedly Nonmagnetic Osmium Oxide, Phys. Rev. Lett. 133, 066501 (2024).
- [12] F. I. Frontini, G. H. J. Johnstone, N. Iwahara, P. Bhattacharyya, N. A. Bogdanov, L. Hozoi, M. H. Upton, D. M. Casa, D. Hirai, and Y.-J. Kim, Spin-orbit-lattice entangled state in a₂mgreo₆ (A = Ca, sr, ba) revealed by resonant inelastic x-ray scattering, Phys. Rev. Lett. 133, 036501 (2024).
- [13] J. Soh, M. E. Merkel, L. V. Pourovskii, I. Živković, O. Malanyuk, J. Pásztorová, S. Francoual, D. Hirai, A. Urru, D. Tolj, D. F. Mosca, O. V. Yazyev, N. A. Spaldin, C. Ederer, and H. M. Rønnow, Spectroscopic signatures and origin of hidden order in Ba₂MgReO₆,

- Nat. Commun. 15, 10383 (2024).
- [14] I. Živković, J. Soh, O. Malanyuk, R. Yadav, F. Pisani, A. M. Tehrani, D. Tolj, J. Pásztorová, D. Hirai, Y. Wei, W. Zhang, C. Galdino, T. Yu, K. I. Ishii, A. Demuer, O. V. Yazyev, T. Schmitt, and H. M. Rønnow, Dynamic jahn-teller effect in the strong spin-orbit coupling regime, Nat. Commun. 15, 8587 (2024).
- [15] A. Nicholls, J.-R. Soh, Y. Yang, A. Bombardi, D. Hirai, H. M. Rønnow, and I. Živković, Evidence of rotational and tilting disorder of ReO₆ octahedra in single crystals of a 5d¹ double perovskite Ba₂CaReO₆, J. Magn. Magn. Mater **632**, 173516 (2025).
- [16] T. Muroi, D. Hirai, H. Sagayama, T.-h. Arima, and Z. Hiroi, Magnetic field-induced tetragonal domain alignment and structural distortion in the spin-orbit-coupled insulator Ba₂MgReO₆, Phys. Rev. Mater. 9, 084415 (2025).
- [17] K. Shibuya, D. Hirai, and K. Takenaka, Chemical pressure tuning of multipolar and magnetic orders in $\rm Ba_2(Cd_{1-x}Ca_x)ReO_6$ double perovskites, Phys. Rev. Mater. 9, 034406 (2025).
- [18] N. Iwahara, J. Soh, D. Hirai, I. Živković, Y. Wei, W. Zhang, C. Galdino, T. Yu, K. Ishii, F. Pisani, O. Malanyuk, T. Schmitt, and H. M. Rønnow, Persisting quantum vibronic dynamics in a 5d¹ double perovskite oxide, Phys. Rev. B 112, 104104 (2025).
- [19] C. A. Marjerrison, C. M. Thompson, G. Sala, D. D. Maharaj, E. Kermarrec, Y. Cai, A. M. Hallas, M. N. Wilson, T. J. S. Munsie, G. E. Granroth, R. Flacau, J. E. Greedan, B. D. Gaulin, and G. M. Luke, Cubic Re^{6+} (5d¹) Double Perovskites, $\mathrm{Ba_2MgReO_6}$, $\mathrm{Ba_2ZnReO_6}$, and $\mathrm{Ba_2Y_2/_3ReO_6}$: Magnetism, Heat Capacity, $\mu\mathrm{SR}$, and Neutron Scattering Studies and Comparison with Theory, Inorg. Chem. 55, 10701 (2016).
- [20] C. J. Ballhausen, Introduction to Ligand Field Theory (McGraw-Hill, 1962).
- [21] G. L. Stamokostas and G. A. Fiete, Mixing of $t_{2g} e_g$ orbitals in 4d and 5d transition metal oxides, Phys. Rev. B **97**, 085150 (2018).
- [22] J. S. Griffith, The Theory of Transition-Metal Ions (Cambridge University Press, 1961).
- [23] M. Mitrano, S. Johnston, Y.-J. Kim, and M. P. M. Dean, Exploring Quantum Materials with Resonant Inelastic X-Ray Scattering, Phys. Rev. X 14, 040501 (2024).
- [24] J. F. Pérez-Torres, Relativistic Effects in Ligand Field Theory (I): Optical Properties of d¹ Atoms in O'_h Symmetry, Inorg. Chem. 63, 15016 (2024).
- [25] J. F. Pérez-Torres, Relativistic Effects in Ligand Field Theory (II): Optical and Magnetic Properties of d¹ Atoms in Cubic and Tetragonal Symmetries, J. Phys. Chem. A 129, 3844 (2025).
- [26] M. Nakahara and T. Ohmi, Quantum Computing: from Linear Algebra to Physical Realizations (Taylor & Francis, 2008).

- [27] F. Roósz and K. Held, Density matrix of electrons coupled to Einstein phonons and the electron-phonon entanglement content of excited states, Phys. Rev. B 106, 195404 (2022).
- [28] J. L. Sanz-Vicario, J. F. Pérez-Torres, and G. Moreno-Polo, Electronic-nuclear entanglement in ${\rm H_2}^+$: Schmidt decomposition of non-Born-Oppenheimer wave functions expanded in nonorthogonal basis sets, Phys. Rev. A **96**, 022503 (2017).
- [29] M. Blavier, R. D. Levine, and F. Remacle, Time evolution of entanglement of electrons and nuclei and partial traces in ultrafast photochemistry, Phys. Chem. Chem. Phys. 24, 17516 (2022).
- [30] A. Palii, S. Aldoshin, B. Tsukerblat, J. J. Borràs-Almenar, J. M. Clemente-Juan, S. Cardona-Serra, and E. Coronado, Electric Field Generation and Control of Bipartite Quantum Entanglement between Electronic Spins in Mixed Valence Polyoxovanadate $[{\rm GeV}_{14}{\rm O}_{40}]^{8-}$, Inorg. Chem. **56**, 9547 (2017).
- [31] D. Materia, L. Ratini, C. Angeli, and L. Guidoni, Quantum information reveals that orbital-wise correlation is essentially classical in natural orbitals, J. Chem. Phys. 161, 244108 (2024).
- [32] G. Greene-Diniz, C. N. Self, M. Krompiec, L. Coopmans, M. Benedetti, D. M. noz Ramos, and M. Rosenkranz, Measuring correlation and entanglement between molecular orbitals on a trapped-ion quantum computer, Sci. Rep. 15, 28409 (2025).
- [33] W. L. You, A. M. Oleś, and P. Horsch, Entanglement driven phase transitions in spin-orbital models, New J. Phys. 17, 083009 (2015).
- [34] R. Safaiee and M. M. Golshan, Von Neumann entropy in a Rashba-Dresselhaus nanodot; dynamical electronic spin-orbit entanglement, Eur. Phys. J. B 90, 121 (2020).
- [35] J. M. Tang, Q. S. Zeng, and Y. B. Luo, The relationship between single-particle commuting observables l_z , s_z entangled states and the spin-orbit coupling, Quantum Inf. Process 19, 40 (2020).
- [36] D. Gotfryd, E. M. Pärschke, J. Chaloupka, A. M. Oleś, and K. Wohlfeld, How spin-orbital entanglement depends on the spin-orbit coupling in a Mott insulator, Phys. Rev. Res. 2, 0133353 (2020).
- [37] T. Sugano, Y. Tanabe, and H. Kamimura, Multiplets of Transition-Metals Ions in Crystals (Academic Press, 1970).
- [38] W. Greiner, Relativistic Quantum Mechanics: Wave Equations, 3rd ed. (Springer, Berlin, 2000).
- [39] H. Bethe, Termaufspaltung in Kristallen, Annalen der Physik 395, 133 (1929).
- [40] W. Moffitt, G. L. Goodman, M. Fred, and B. Weinstock, The colours of transition metals hexafluorides, Mol. Phys. 2, 109 (1959).
- [41] M. Rotger, V. Boudon, and H. Selig, Absorption spectrum of the $a(E'_{2g}) \leftarrow X(G'_g)$ and $b(G'_g) \leftarrow X(G'_g)$ electronic transition of ReF₆, Spectrochim. Acta A **55**, 1575 (1999).

- [42] H. Selig, F. A. Cafasso, D. M. Gruen, and J. G. Malm, Magnetic Susceptibility of ReF₆, J. Chem. Phys. 36, 3440 (1962).
- [43] K. Stitzer, M. K. Smith, and H.-C. zur Loye, Crystal growth of Ba₂MOsO₆ (M=Li, Na) from reactive hydroxide fluxes, Solid State Science 4, 311 (2002).
- [44] J. H. V. Vleck, Quantum Mechanics: The Key to Understanding Magnetism, Science 201, 113 (1978).
- [45] M. E. Merkel, A. M. Tehrani, and C. Ederer, Probing the mott insulating behavior of Ba₂MgReO₆ with DFT+ DMFT, Phys. Rev. Res. 6, 023233 (2024).
- [46] D. Fiore-Mosca, H. Schnait, L. Celiberti, M. Aichhorn, and C. Franchini, The Mott transition in the 5d¹ compound Ba₂NaOsO₆: A DFT+DMFT study with PAW spinor projectors, Comput. Mater. Sci. 233, 112764 (2024).
- [47] A. Sunaga, Structure and Excitation Spectra of Third-Row Transition Metal Hexafluorides Based on Multi-Reference Exact Two-Component Theory, Inorg. Chem. 63, 18335 (2024).
- [48] D. A. Kukusta, L. V. Bekenov, and V. N. Antonov, Resonant inelastic x-ray scattering in double perovskites from first-principles. I. A₂YReO₆ (A = Ba and Sr), J. Magn. Magn. Mater 614, 172714 (2025).
- [49] J. Okamoto, G. Shibata, Y. S. Ponosov, H. Hayashi, K. Yamaura, H. Y. Huang, A. Shing, C. T. Cheng, A. Tanaka, S. V. Streltsov, D. J. Huang, and A. Fujimori, Spin-orbit-entangled state of Ba₂CaOsO₆ studied by O K-edge resonant inelastic X-ray scattering and Raman spectroscopy, npj Quantum Mat. 10, 44 (2025).
- [50] M. W. Haverkort, M. Zwierzycki, and O. K. Andersen, Multiplet ligand-field theory using Wannier orbitals, Phys. Rev. B 85, 165113 (2012).
- [51] J. Jung, M. Atanasov, and F. Neese, Ab Initio Ligand-Field Theory Analysis and Covalency Trends in Actinide and Lanthanide Free Ions and Octahedral Complexes, Inorg. Chem. 56, 8802 (2017).
- [52] S. K. Singh, J. Eng, M. Atanasov, and F. Neese, Covalency and chemical bonding in transition metal complexes: An ab initio based ligand field perspective, Coordination Chemistry Reviews 344, 2 (2017).
- [53] S. V. Rao, D. Maganas, K. Sivalingam, M. Atanasov, and F. Neese, Extended Active Space Ab Initio Ligand Field Theory: Applications to Transition-Metal Ions, Inorg. Chem. 63, 24672 (2024).
- [54] C. A. Cardot, J. J. Kas, J. E. Abramson, J. J. Rehr, and G. T. Seidler, Core-to-core X-ray emission spectra from Wannier based multiplet ligand field theory, J. of Electron Spectroscopy and Related Phenomena 270, 147419 (2024).
- [55] V. R. M. Nielsen, M. Grasser, B. Le Guennic, and T. J. Sørensen, Neodymium(III) Aqua Ion as a Model System in Ab Initio Crystal Field Analysis Beyond Point Charges and Crystal Field Theory, Inorg. Chem. 64, 3463 (2025).